A Method for Superelastic Constitutive Properties Calibration Using Full-field Surface Strain Data

Harshad M. Paranjape[a,*], Kenneth I. Aycock[b], Craig Bonsignore[a], Jason D. Weaver[b], Brent A. Craven[b], Thomas W. Duerig[a]

[a]*Confluent Medical Technologies, Inc. 47533 Westinghouse Drive, Fremont, CA 94539, United States.*
[b]*U.S. Food and Drug Administration, Center for Devices and Radiological Health, Office of Science and Engineering Laboratories, Division of Applied Mechanics., Silver Spring, MD 20993, United States.*

Abstract

Superelastic Nitinol is a widely used material to manufacture implantable medical devices. Simulations are extensively used in the design, optimization, and durability assessment of Nitinol implants. The constitutive response of superelastic materials is non-linear, anisotropic, and asymmetric in tension vs. compression. The existing methods to determine the superelastic material properties used in finite element simulations typically do not account for some of these complexities. The goal of this work is to introduce a method to determine the superelastic material constitutive properties using full-field surface strain measurements. We propose using digital image correlation to obtain surface strain fields during tensile testing of specially designed diamond specimens. The material properties are determined by minimizing a difference metric defined in terms of the local strain difference and the global load difference between the experiment and trial simulations. We also propose a metric in terms of the local strain difference between experimental measurement and simulation prediction to report the credibility of the material properties fitted using this method. The philosophy behind this method and the proposed metric to quantify the accuracy of material property fitting reflects the growing consensus in the implantable device community that the simulation results must be accompanied by a quantification of their credibility.

Keywords: Superelasticity, NiTi, Shape Memory Alloys, Finite Element Modeling, Digital Image Correlation

1. Introduction

Medical implants undergo deformation during manufacturing, during deployment in the human body, and in their implanted state. When implanted, these devices can undergo cyclic deformation due to biomechanical processes such as walking, breathing, and cardiac rhythm [1]. Computer simulations are extensively used to predict the deformation in implants during all of these states. For example, finite element modeling (FEM) simulations are used to estimate the mean stress or strain and the alternating stress or strain in the implants due to cyclic loading in the human body.

Nitinol is a widely used material to manufacture medical devices [2]. Typically, superelastic Nitinol is used to manufacture implants since it furnishes large recoverable strains at body temperature due to an austenite to martensite phase transformation. Simulations are extensively used in the design and optimization of Nitinol implants. Simulation of Nitinol deformation is particularly challenging because the constitutive response of superelastic Nitinol is highly nonlinear, anisotropic [3], and asymmetric in tension vs. compression [4, 5]. A typical stress-strain curve for Nitinol is shown in Figure 1. The stress-strain response can be adequately described in terms of six key material parameters: (1) Austenite elastic stiffness

*Corresponding author
Email address: harshad.paranjape@confluentmedical.com (Harshad M. Paranjape)

(E_A). (2) Martensite elastic stiffness (E_M). (3) Upper plateau stress for phase transformation (UPS), (4) Lower plateau stress (LPS). (5) Transformation strain during tensile loading (etr). (6) Transformation onset stress in compression (CPS).

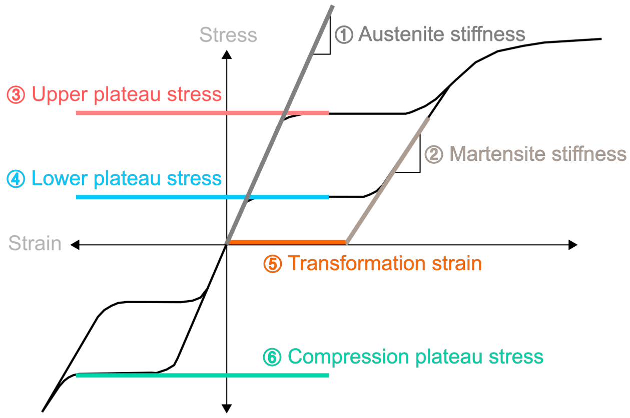

Figure 1: A schematic of the typical stress-strain response of superelastic Nitinol. The behavior can be described in terms of six key material parameters that annotated in the stress-strain curve.

A prerequisite to performing simulations of Nitinol deformation is the knowledge of constitutive properties of Nitinol. For example, to perform Nitinol simulations in Abaqus FEM framework, the six key material parameters are determined by utilizing experimental stress-strain data for the appropriate Nitinol raw material. A typical method to determine the material property is to perform a tensile test on Nitinol tube, wire, or strip of interest and determine the Nitinol FEM material properties using either a manual parameter extraction approach or using a semi-supervised computer program. A key disadvantage of this approach is that the constitutive response of Nitinol is determined using tensile data only. However, in implants such as stents, the deformation is bending dominated. Also, it is challenging to quantify the uncertainty in the determined material properties using this method. Arguably, one can perform several tensile tests, fit material properties to those data, and then report the mean and standard deviation of the fitted properties. However, this approach never quantifies the accuracy of local strains predicted by the fitted material properties. This deficiency in turn can be addressed by performing separate validation studies. However, there is an opportunity to develop a standardized single test method that can be used to determine the constitutive properties of Nitinol and also quantify the accuracy of the fitted material properties.

Recently, several full-field strain characterization methods have become available. Digital image correlation (DIC) is one such method that can furnish full-field surface strain fields during mechanical testing of materials including Nitinol. Some prior efforts have sought to utilize DIC to calibrate elasto-plastic material properties [6–8]. However, no such approach exists for Nitinol. Thus, we propose a test method to determine Nitinol constitutive properties used in FEM using DIC measurements. The test method and data analysis is described in the Methods section. Some key results are summarized in the Results and Discussion section.

2. Methods

We designed a diamond shaped specimen, schematically shown in Figure 2(a). We manufactured the diamond specimens from Ti-50.8at.%Ni material strip using laser cutting. We heat treated the specimen such that the M^* temperature was below the room temperature and thus the material was superelastic at room temperature. We electropolished the specimens to give smooth surface finish.We applied a thin coat of matte white spray paint to the surface of the diamond gage section. We created a high-contrast speckle pattern on the surface of the specimens by applying finely ground charcoal pattern. A representative speckle pattern is shown in Figure 2(b). The white-to-black area ratio after applying the speckle pattern was approximately 0.5. The speckle pattern is required for performing the DIC measurements.

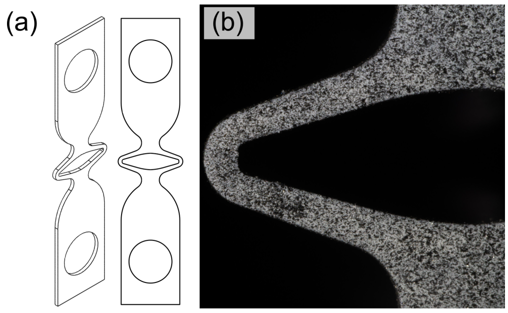

Figure 2: Specimen geometry. (a) A schematic of the diamond-shaped specimen used in this study. (b) A representative speckle pattern applied on the surface of the specimen for performing DIC measurements.

We performed a tensile test on the specimen using an Instron 5969 load frame with 1 kN load cell. The test was performed at room temperature, in displacement control, at a nominal displacement rate of $3.3 \times 10^{-3}\,\mathrm{mm\,s^{-1}}$. The specimen was loaded to a peak displacement of 0.2 mm, unloaded to 0.1 mm, then reloaded to 0.2 mm, and finally unloaded to zero load as shown in Figure 4(a). To measure the full-field surface strains in the gage of the diamond specimens during tensile testing, we performed DIC measurements during the tensile test. For this, we setup a Sony A7III digital camera with a Mitakon Zhongyi 20 mm f/2 4.5X Super Macro lens in front of the load frame as schematically shown in Figure 3. We illuminated the specimen using an LED light such that the speckle pattern can be photographed using an exposure time of approximately 0.2 s at ISO 400. We recorded images with the camera at regular intervals such that images were available at the peak displacement and on unloading to 0.1 mm displacement.

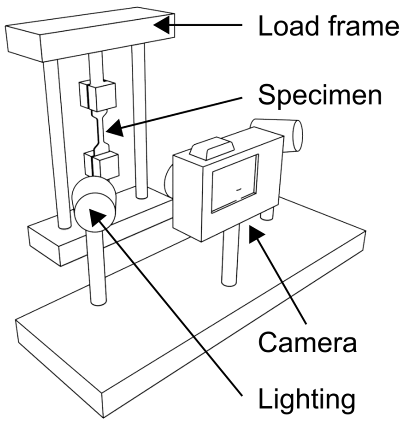

Figure 3: A schematic of the DIC setup.

We determined the surface strains by analyzing the digital camera images using the NCORR 2D DIC software [9]. We processed only one quarter of the diamond gage section because of the symmetry in the geometry with respect to the loading condition. We used a subset size of 30. An example of the strains extracted from DIC measurements in the diamond is shown in Figure 4(b). NCORR software furnishes Green-Lagrange strains.

We created a simulation of the diamond specimen geometry being loaded in tension with identical test parameters as those in the tensile test. The model is shown in Figure 5. We simulated one quarter of the diamond geometry considering the symmetry. We created baseline version of the simulation using representative Nitinol material properties. Then, using an automated computer script, we created 1200 simulations with slightly perturbed six material properties listed in Section 1. To create the matrix of 1200

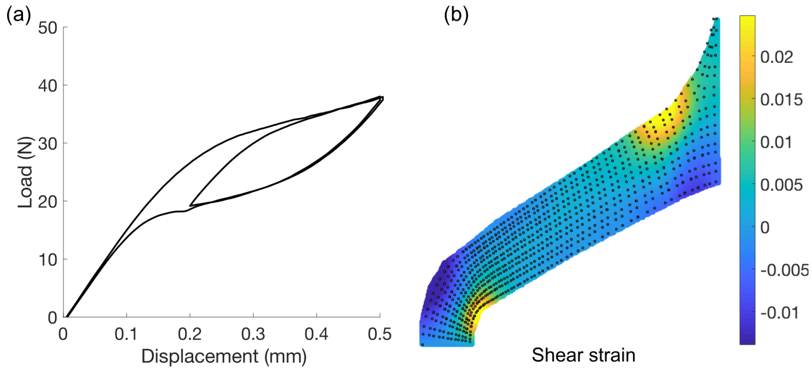

Figure 4: Load and strain response during tensile test. (a) Load-displacement curve for the tensile test. (b) Surface shear strain obtained from DIC

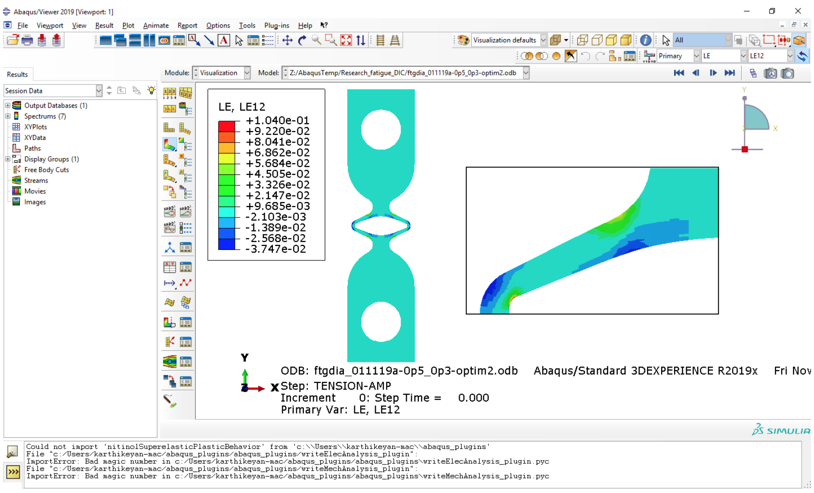

Figure 5: Finite element model setup. The strains obtained using FEM are shown in the inset.

perturbed material properties, we chose reasonable extrema for each property (e.g., UPS is typically between 200 MPa and 800 MPa) and then used Latin hypercube sampling to create the perturbed values. We did not consider unphysical parameter combinations such as martensite stiffness being larger than austenite stiffness, difference in the upper and lower plateaus being smaller than 100 MPa, and compression plateau stress being less in magnitude compared to the upper plateau stress. These assumptions are reasonable for the rolled strip Nitinol material used in this study. We ran the simulations using a batch processor on a 16-core high-performance computing system. We used Abaqus/Standard 2019 FEM framework to run the simulations. We post-processed the 1200 simulations to obtain the local shear strains in the diamond gage at the peak displacement and after unloading to 0.1 mm displacement. We also extracted the global load-displacement response for each simulation.

We developed a Matlab-based computer program to compare the local shear strain field from DIC to that from FEM simulations and to compare the load-displacement response between the tensile test and FEA as shown in Figure 6(a-d). We compared the shear strain at four key points in the diamond gage geometry. We performed this comparison at a displacement of 0.2 mm and 0.1 mm as described above. We compared the load at two key points. We performed the strain and load comparison at 0.1 mm displacement because it is essential to compare the response during unloading to determine the lower plateau stress (LPS). We performed the strain comparison at four key points. To make the strain comparison, we smoothed the DIC and FEM strain fields using linear interpolation to a common grid such that the spatial resolution of the data was comparable between the two strain fields.

We defined a metric to quantify the difference between FEM and DIC. The metric consisted of two contributions: (1) The absolute value of difference between the strains at four key points at displacements of 0.2 mm 0.1 mm, normalized by the maximum strain in the four key points of interest. (2) The absolute value of load difference at two key points, normalized by the load values in the tensile test at each of the points. The normalization of each contribution is essential considering that the load values are of the order of 10^1 and the strain values are of the order of 10^{-2}. Thus, this exercise furnished 1200 values for the difference metric from 1200 simulations. Note that the difference metric is unit less because of the normalization.

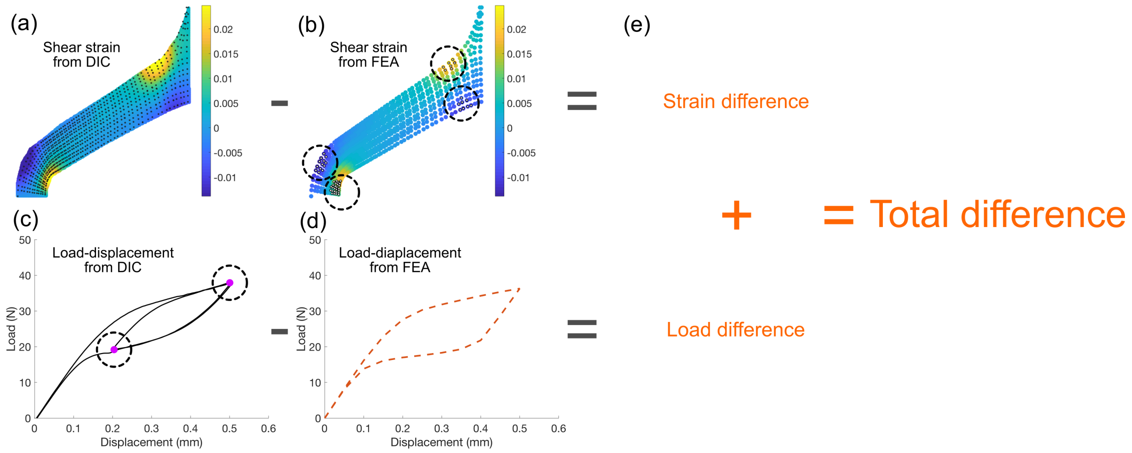

Figure 6: FEM and DIC comparison. (a) Shear strain from DIC. (b) Shear strain from FEM at peak load. The strain comparison is performed at four key areas shown by circles. (c) Load-displacement from the tensile test. (d) Load-displacement from FEM. The load comparison is performed at two key points shown by circles. (e) The difference metric quantifying the load and strain difference between FEA and DIC.

3. Results and Discussion

The variation in the difference metric as a function of each of the six Nitinol material parameters is shown in Figure 7. It can be seen that the difference metric is sensitive to austenite stiffness, lower plateau stress, and compression plateau stress. It is weakly sensitive to upper plateau stress. And, it is insensitive to the martensite stiffness and transformation strain. For the deformation that we imposed on the diamond, the response of the majority of the gage section remained that of austenite elasticity as seen in the strain field in Figure 4(b). Thus, it is natural that the response is sensitive to austenite stiffness variation. The imposed displacement was not large enough to cause substantial volume to fully transform to martensite and then deform through martensite elasticity. This rationalizes the insensitivity of results to martensite stiffness and transformation strain parameters. Two out of the four regions selected for strain comparison deformed in compression (extrados at the apex and the introduce near the grip). This is likely the reason behind the response being sensitive to compression plateau.

From these results, we selected the material parameters that furnished the smallest difference metric. We created a new FEM simulation with these properties and compared the output with tensile test data and DIC outputs. The difference in the local shear strain prediction from these optimized material properties and the DIC measurements is shown in Figure 8(a). Note that the maximum DIC strain at the intrados was 0.025. Overall, FEM underestimated the strains in the regions where tensile deformation occurred (intrados at the diamond apex and extrados near the grip). In the compressive regions, the fit is better. A comparison of the load-displacement responses between the tensile test and the simulation with optimized material parameters is shown in Figure 8(b). There is a remarkable similarity in the simulation and the experiment.

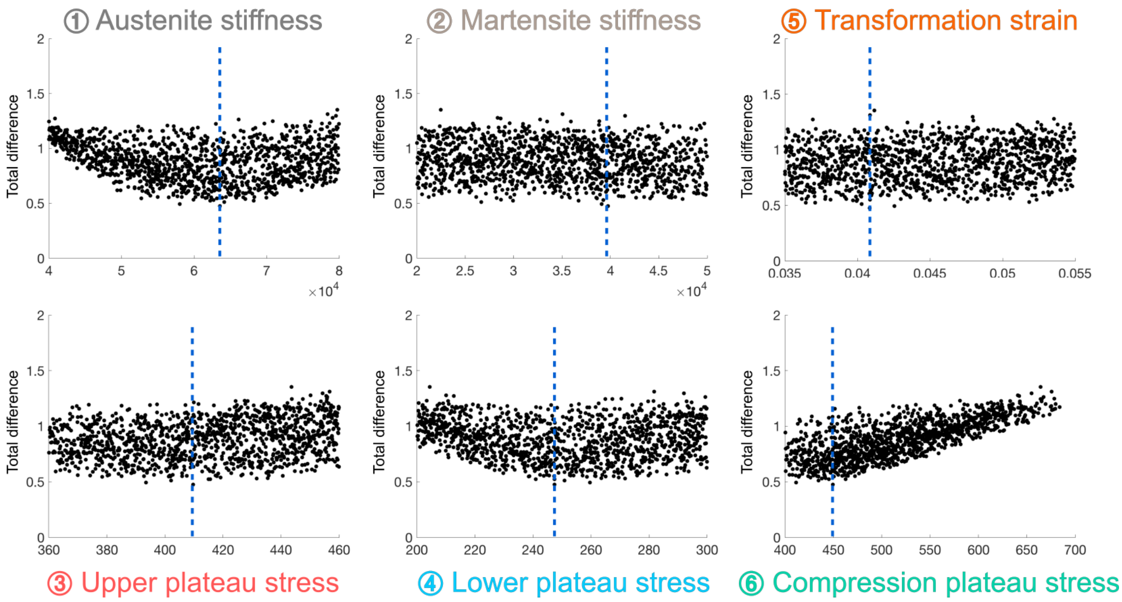

Figure 7: Scatter plots of the difference metric plotted against each of the six Nitinol Abaqus material parameters for the 1200 simulation cases. The parameters furnishing the smallest error are shown by vertical dashed line.

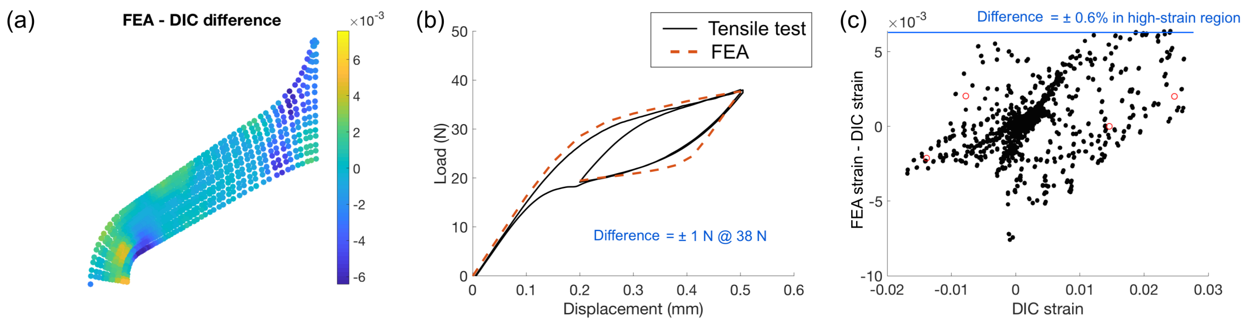

Figure 8: DIC and FEA comparison from the determined material properties that minimized the difference metric. (a) Local strain field difference. (b) Load-displacement comparison. (c) A proposed material property fit accuracy metric in terms of the maximum difference in local strain prediction and experimental ground truth.

When Nitinol material properties for FEM are determined, a validation study is performed. Typically, the load-displacement response from the experiment used for validation serves as a comparator and the accuracy of material property determination is reported in terms of the difference in the simulated load and the comparator. This accuracy metric is annotated in Figure 8(b). Here we compared the experimental load-displacement curve for the diamond with the simulated resposne from optimum material properties. In terms of this metric, the fit achieved through this material property determination scheme is quite satisfactory. However, typically, Nitinol simulations are performed to determine the worst-case local strains. For example, largest strains during implant deployment from a catheter are simulated to assess the possibility of introducing a permanent set. Largest mean strain and strain amplitude during cyclic loading are simulated to determine the worst-case fatigue loading conditions. Thus, an accuracy metric that is more aware of the differences in the local strain predictions from the experimental ground truth would be more useful. Thus, we propose that it would be more appropriate to report the difference in the local strain prediction and corresponding experimental measurement in order to quantify the accuracy of the material property determination. An example of this is shown in Figure 8(c). The optimized material properties in this study, furnished local strains within an accuracy of $\pm 0.6\%$ in the high-strain regions.

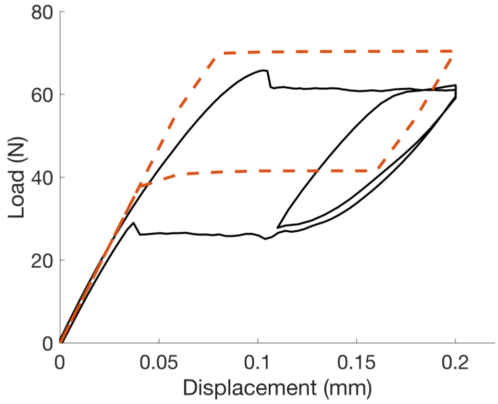

Figure 9: A comparison of the tensile response simulated from the optimized material properties determined in this study and a tensile test on a dogbone. The simulation data are shown by the dashed curve. The simulation over-predicted the plateaus in tensile loading.

To assess the performance of these optimized material properties in other deformation modes such as axial loading, we performed a tensile test on a dogbone specimen. We created a simulation of the dogbone tensile loading and compared the load-displacement response from the simulation to that in the experiment. The comparison is shown in Figure 9. These material properties overestimated the plateaus in the tensile loading mode. Thus, in practice, any material property determination schemes such as the one described here may have to rely on experimental data from more than one deformation mode.

4. Summary

We proposed a method to determine the Nitinol FEM constitutive properties by utilizing full-field surface strain data obtained during the tensile testing of a diamond specimen. We used DIC to experimentally obtain the strain fields. We defined a metric to quantify the difference between experiments and the simulations in terms of the local strains in key areas and global load at key points along the load-displacement curve. We determined the optimum material properties by creating simulations with perturbed material constants and selecting the material parameters that minimized the difference metric. The optimum Nitinol material properties determined using this scheme furnished a good match to the experimentally measured load-displacement response of a diamond specimen, furnished a reasonable match with the locally measured strains, and furnished poor comparison with the tensile load-displacement response of a dogbone specimen. We argued that reporting the accuracy of the material property fitting in terms of the largest difference in the local strain prediction would be more useful with respect to the typical use cases of Nitinol deformation simulations.

The method proposed in this study would be useful to the medical implant community considering the increasing reliance on simulations in the implant design, optimization, and durability assessment. The philosophy behind the proposed metric to quantify the accuracy of material property fitting here reflects the growing consensus that the simulation results must be accompanied by a quantification of their credibility [10].

Future improvements to this fitting scheme include the development of a statistical optimization model that would allow calculation of the optimum material properties from a few simulations rather than hundreds of trial simulations. Improvement to loading condition or specimen geometry can be made to increase the gage volume that undergoes phase transformation and furnished larger strains. These changes could increase the accuracy of fitting.

Acknowledgements

HMP is grateful to Confluent Medical Technologies, Inc. for funding this work. HMP would like to thank Bill Ng and Lot Vien (Confluent) for assistance with sample preparation and testing. The diamond specimen geometry specification is available on request.

References

[1] C. Cheng (Ed.), Handbook of Vascular Motion, 1 ed., Academic Press, 2019.
[2] T. Duerig, A. Pelton, D. Stöckel, Materials Science and Engineering: A 273-275 (1999) 149–160. doi:10.1016/S0921-5093(99)00294-4.
[3] J. McNaney, V. Imbeni, Y. Jung, P. Papadopoulos, R. Ritchie, Mechanics of Materials 35 (2003) 969–986. doi:10.1016/S0167-6636(02)00310-1.
[4] K. Gall, H. Sehitoglu, Y. Chumlyakov, I. Kireeva, Acta Materialia 47 (1999) 1203–1217. doi:10.1016/S1359-6454(98)00432-7.
[5] K. Gall, International Journal of Plasticity 15 (1999) 69–92. doi:10.1016/S0749-6419(98)00060-6.
[6] A. P. Ruybalid, J. P. M. Hoefnagels, O. v. d. Sluis, M. G. D. Geers, International Journal for Numerical Methods in Engineering 106 (2016) 298–320. doi:10.1002/nme.5127.
[7] M. Bertin, C. Du, J. P. Hoefnagels, F. Hild, Acta Materialia 116 (2016) 321–331. doi:10.1016/j.actamat.2016.06.039.
[8] Z. Zhang, B. Pan, M. Grédiac, W. Song, Optics and Lasers in Engineering 103 (2018) 55–64. doi:10.1016/j.optlaseng.2017.11.016.
[9] J. Blaber, B. Adair, A. Antoniou, Experimental Mechanics 55 (2015) 1105–1122. doi:10.1007/s11340-015-0009-1.
[10] ASME V&V40-2018, Assessing Credibility of Computational Modeling Through Verification and Validation: Application to Medical Devices, Standard, 2018.